AGU PUBLICATIONS

Tectonics

RESEARCH ARTICLE
10.1002/2017TC004696

Key Points:
- Early Paleozoic rift in East Gondwana involved denudation of Proterozoic Pinjarra Orogen and Archean Yilgarn Craton basement
- Northampton Complex (Pinjarra Orogen) constituted a basement high that separated subbasins during the onset of rifting
- Detrital zircon age spectra constrain West Australian Craton and North Indian provenance for continental red beds

Supporting Information:
- Supporting Information S1
- Table S1

Correspondence to:
V. Markwitz,
vanessa.markwitz@research.uwa.edu.au

Citation:
Markwitz, V., Kirkland, C. L., Wyrwoll, K.-H., Hancock, E. A., Evans, N. J., & Lu, Y. (2017). Variations in zircon provenance constrain age and geometry of an Early Paleozoic rift in the Pinjarra Orogen, East Gondwana. *Tectonics*, *36*, 2477–2496. https://doi.org/10.1002/2017TC004696

Received 16 JUN 2017
Accepted 18 OCT 2017
Accepted article online 25 OCT 2017
Published online 13 NOV 2017

Variations in Zircon Provenance Constrain Age and Geometry of an Early Paleozoic Rift in the Pinjarra Orogen, East Gondwana

V. Markwitz[1], C. L. Kirkland[2,3], K.-H. Wyrwoll[1], E. A. Hancock[4], N. J. Evans[3], and Y. Lu[4,5]

[1]School of Earth Sciences, The University of Western Australia, Crawley, WA, Australia, [2]Centre for Exploration Targeting—Curtin Node, Curtin University, Perth, WA, Australia, [3]John de Laeter Centre, TIGeR, Department Applied Geology, Curtin University, Perth, WA, Australia, [4]Geological Survey of Western Australia, Perth, WA, Australia, [5]Centre for Exploration Targeting and Australian Research Council Centre of Excellence for Core to Crust Fluid Systems (CCFS), School of Earth Sciences, The University of Western Australia, Crawley, WA, Australia

Abstract The Tumblagooda Sandstone in Western Australia documents Early Paleozoic rifting in East Gondwana and provides the earliest evidence for terrestrial activity of multicellular animals on Earth. We constrain the provenance of this sequence using 737 concordant U–Pb ages of detrital zircons from two stratigraphic wells in the northern Perth Basin and Southern Carnarvon Basin and outcrops of the type sections near Kalbarri. Detrital zircon age signatures are linked to infrared spectral data and stratigraphic logs. These ages span 3,312–466 Ma, including major Precambrian age peaks at 1,079–1,544 Ma, 1,695–2,403 Ma, and 2,640–2,879 Ma, consistent with igneous sources in the West Australian Craton. Significant Early Paleozoic age peaks at 499–541 Ma suggest a North Indian Orogen source. The maximum depositional age is constrained by the youngest detrital zircon, which yields an age of 466 ± 8 Ma. Our age constraints imply that terrestrial activity of multicellular animals on Earth may not be older than Middle Ordovician (Darriwilian). Rifting resulted in the exposure of the Yilgarn Craton and the segmentation of the Pinjarra Orogen. The Northampton Complex segment of the Pinjarra Orogen constituted a basement high that separated subbasins during the onset of rifting. Discordant Archean zircons provide a consistent record of radiogenic Pb loss at ~470 Ma, which we interpret as being related to the denudation of the Yilgarn Craton. The Pb loss event suggests that intracratonic rifting in the Pinjarra Orogen was initiated in the Middle Ordovician, after the Kuunga Orogeny completed the final amalgamation of Gondwana.

1. Introduction

Provenance studies often rely on U–Pb zircon geochronology because zircon grains resist a wide range of physical and chemical alteration processes and are able to survive multiple erosion and redeposition cycles (Fedo, Sircombe, & Rainbird, 2003). Chemically unstable heavy minerals are selectively removed from heavy mineral assemblages during diagenesis, once the burial depth exceeds ~2 km (Morton, 1986; Walderhaug & Porten, 2007). This includes garnet, titanite, epidote, pyroxene, and tourmaline, all of which are highly susceptible to alteration and preferential dissolution (Walderhaug & Porten, 2007). Therefore, detrital zircon geochronology can be a powerful tool in basin evolution studies to link sink to source regions (e.g., Andersen, 2005; Cawood et al., 2003; Moecher & Samson, 2006; Thomas, 2011; Veevers et al., 2005), particularly when applied within the context of stratigraphic control.

The Tumblagooda Sandstone documents Early Paleozoic rifting in East Gondwana and is known for preserving some of the earliest evidence for complex terrestrial communities in the fossil record (McNamara, 2014; Ortega-Hernández et al., 2010; Trewin & McNamara, 1995). Despite its importance, the age of the Tumblagooda Sandstone is poorly constrained with age estimates ranging from Cambrian to Devonian based on trace fossil assemblages, stratigraphy ,and paleomagnetic analyses (e.g., Hocking, 1987; McNamara, 2014; Playford et al., 1976; Schmidt & Embleton, 1990). Previous provenance studies based their interpretations on relatively few samples that were widely distributed across the succession. Cawood and Nemchin (2000) interpreted the provenance of the Perth Basin that continues south of the Southern Carnarvon Basin and contains predominantly Permian-Quaternary age strata. The Tumblagooda Sandstone overlays the northern part of the Perth Basin's basement. For one Tumblagooda Sandstone sample taken east of the Northampton Complex, Cawood and Nemchin (2000) reported Early Paleozoic to Archean U–Pb zircon

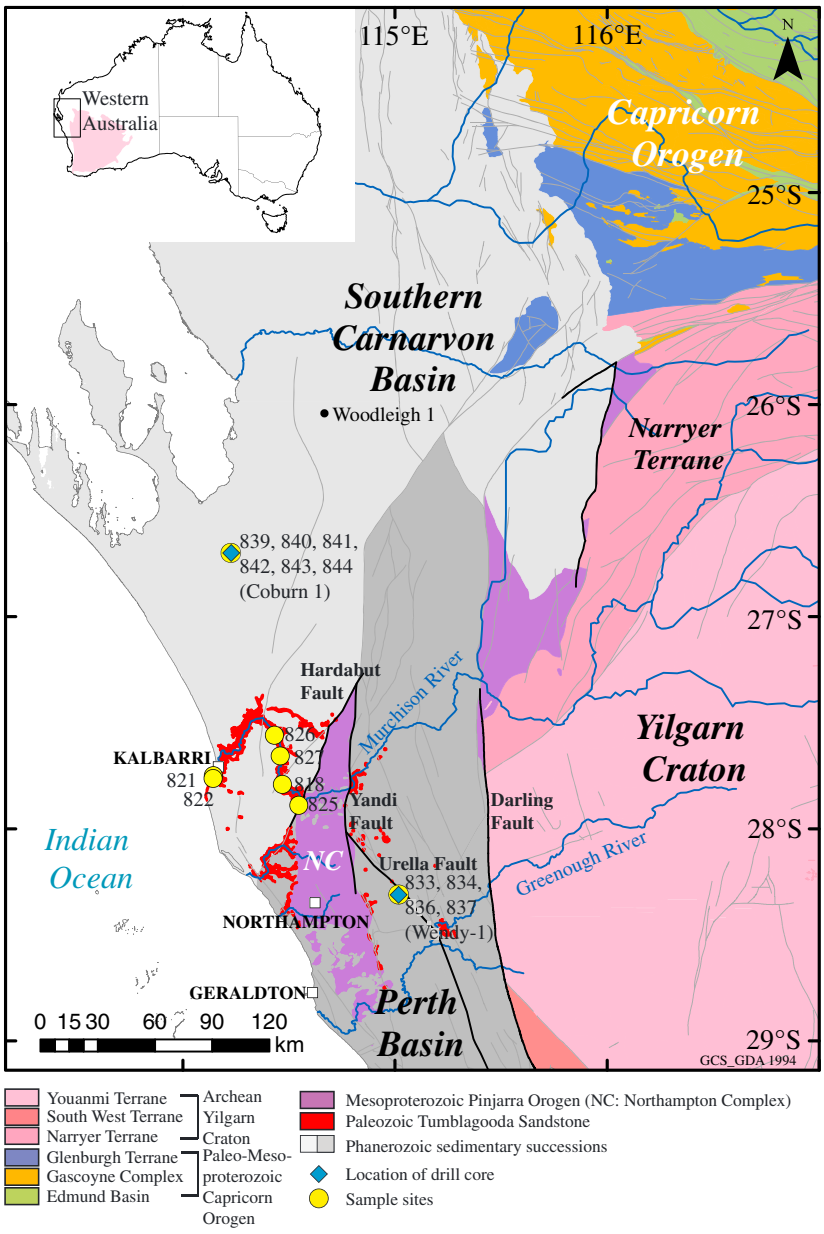

Figure 1. Geological map and locations of drill cores and sample sites. Outcrop of the Tumblagooda Sandstone is shown in red; NC = Northampton Complex (Pinjarra Orogen).

ages. Wingate et al. (2015) and Wingate and Mory (2015) produced similar age spectra to Cawood and Nemchin (2000) from one coastal outcrop sample (Rainbow Valley; same location on the map in Figure 1 than sample 822) and one drill core sample (Coburn 1).

This study reports 737 new concordant U–Pb zircon ages from two drill cores located in the northern Perth Basin and Southern Carnarvon Basin and from six type section samples near Kalbarri (Figure 1). Our objectives were to document important shifts in detrital zircon age spectra relative to stratigraphic position and depositional environment and to constrain age and geometry of an Early Paleozoic rift in the Pinjarra Orogen in East Gondwana. This study identified a complex juxtaposition of Pinjarra Orogen basement segments, resulting in subbasin developments. In addition, the onset of rifting in the Pinjarra Orogen was also accompanied by the denudation of the Archean Yilgarn Craton and the North Indian Orogen.

Due to a lack of datable volcanic marker horizons, younger cross cutting intrusives, and diagenetic phosphate minerals, it is not possible to accurately constrain the age of the Tumblagooda Sandstone. Nonetheless, both

the youngest detrital zircon analyzed (466 ± 8 Ma) and the identification of a major Pb loss event in the source of the Archean detrital zircon population at ~470 Ma provide a similar minimum age constraint for the sediment and therefore limit the age of the Tumblagooda Sandstone to Middle Ordovician (Darriwilian) or younger.

2. Geological Setting

The Southern Carnarvon Basin and northern Perth Basin are located at the west coast of Western Australia and represent an intracratonic rift initiated supposedly in the Cambrian (Veevers et al., 1984) with a major second phase of rifting in the Late Ordovician or Early Silurian (Hocking, 1991). Both basins are bounded to the east by the regional-scale Darling Fault, separating the Archean Yilgarn Craton in the east and Phanerozoic basin sediments in the west. The Tumblagooda Sandstone is a redbed sequence that formed in the Early Paleozoic (Hocking, 1991; Trewin, 1993) and was deposited above basement rocks of the Proterozoic Pinjarra Orogen (Playford et al., 1976; Trewin, 1993; Figure 1), following the Neoproterozoic to Early Cambrian Kuunga Orogeny (Boger, 2011; Collins, 2003; Markwitz et al., 2017; Meert, 2003; Meert & Van Der Voo, 1997).

The assembly of the supercontinent Gondwana followed the breakup of Rodinia between 800 and 700 Ma (e.g., Powell et al., 1993). Eastern Gondwana in the late Neoproterozoic-Cambrian comprised among other cratonic blocks, India, and the adjacent western margin of the Yilgarn Craton (Gregory et al., 2009; Powell & Pisarevsky, 2002). Paleogeographic reconstructions of these cratons and the timing of final Gondwana amalgamation are not well constrained (Gregory et al., 2009, and references therein). Reconstructions of East Gondwana suggest that the Pinjarra Orogen extended into Greater India (Fitzsimons, 2003; Janssen et al., 2003), where the assembly of East Gondwana took place between 750 Ma and 530 Ma (Meert, 2003; Kuunga Orogeny). The Pinjarra Orogen is exposed in at least three highly deformed metamorphic complexes in Western Australia, including the Northampton Complex (Figure 1). The Northampton Complex is bounded by the Hardabut Fault to the west and the Yandi Fault to the east and consists of gneisses, migmatites, granitoids, and dolerite dykes (Myers, 1990) that record an extended magmatic history of granitic intrusions, dyke formation, and of metamorphic events from the Mesoproterozoic to Cambrian (Bruguier et al., 1999; Collins, 2003; Embleton & Schmidt, 1985; Ksienzyk et al., 2012; Markwitz et al., 2017). Rocks of the Pinjarra Orogen recorded a complex tectonometamorphic history including (1) the ~1,090–1,060 Ma Pinjarra Orogeny, which represents the amalgamation of Gondwana; (2) a 1,090–1,020 Ma metamorphic event in the Northampton Complex that apparently postdates the tectonic events in the Albany-Fraser Orogen, the Mawson Craton, and the North Australian Craton (e.g., Goodge et al., 2001; Johnson et al., 2010; Spaggiari et al., 2015); and (3) the ~750–520 Ma Kuunga Orogeny that occurred during the latest stage of amalgamation when India-Africa and Australia-Antarctica collided (Collins, 2003; Markwitz et al., 2017). The Kuunga metamorphic event was identified in Pinjarra Orogen basement rocks of the Leeuwin Complex (Collins, 2003) in the far southwest of Australia and from a previously unconstrained basement domain in the Northampton area, at the base of the Wendy-1 drill core (Markwitz et al., 2017). Several sets of posttectonic pegmatitic dykes intruded the Northampton Complex during the Neoproterozoic at 748 ± 17 Ma and ~550 Ma (Embleton & Schmidt, 1985). Pb vein-type mineralization, which has been dated at 434 ± 16 Ma (Rb-Sr; Richards et al., 1985) is associated with brittle-ductile shear zones (Byrne & Harris, 1993). Detrital zircon ages from paragneisses of the Northampton Complex range between 2,040 Ma and 1,150 Ma, with major age peaks at 1,400–1,150 Ma and 1,900–1,600 Ma (Bruguier et al., 1999; Kriegsman et al., 1999; Ksienzyk et al., 2012). Johnson (2013) argued that the Meso- to Neoproterozoic detrital ages within the basement were similar to basement rocks intersected by the Woodleigh1 drill hole (~300 km north of Northampton; Figure 1), rather than from the much more distal Albany-Fraser Orogen further south. The youngest detrital zircons from a Northampton Complex paragneiss yielded a U–Pb age of 1,150 Ma, which provided a maximum age constraint on these sediments (Bruguier et al., 1999).

Siliciclastic rocks of the Tumblagooda Sandstone were unconformably deposited on Pinjarra Orogen basement rocks over the northern Perth Basin and southern parts of the Southern Carnarvon Basin (Figure 1). The upper boundary of the Tumblagooda Sandstone succession is known from the Coburn 1 drill core as a conformable transition to the Early Silurian Dirk Hartog Formation (Gorter et al., 1994). Allen and Trinajstic

(2017) recently described an Early Devonian fish fauna in Wendy-1 drill core from an unnamed sandstone unit at 368 m above the fluvial facies of the Tumblagooda Sandstone. Tumblagooda Sandstone type section outcrops extend along the Murchison River Gorge and coastal cliffs south of Kalbarri (McWhae et al., 1956), but exposures elsewhere are discontinuous.

A strong alluvial signature of the Tumblagooda Sandstone succession is evident, comprising a red bed sequence of more than 1.5 km in thickness (Hocking, 1991). Sediments were deposited in a braided-fluvial environment in the absence of any vegetation. In contrast to modern fluvial systems, the absence of vegetation at the basin-scale is likely to have resulted in increased sediment erodibility and yield and significantly diminished the development of chemically weathered clays and soils (e.g., Davies & Gibling, 2010). The Tumblagooda Sandstone was deposited on a paleoslope dipping toward the northwest of the basin related to north-south oriented channel systems (Hocking, 1987; Trewin, 1993). Hocking (1987) identified five different facies associations (FA1 to FA5) in measured sections of the Murchison Gorge and coastal cliffs: FA1 and FA3 were deposited in broad braided fluvial settings; FA2 and FA4 represent in tidal environments and FA5 as alluvial fan deposits. Dominant paleocurrent directions for the facies associations are toward the northwest (FA1 and FA3 to F5) and southwest (FA2), with minor fluctuations in directions recognized toward north and west (FA1), southeast (FA2), south and east (FA4), and northeast (FA5).

The Tumblagooda Sandstone is known for abundant trackways from various types of arthropods along with one body fossil of a large amphibious nonmarine euthycarcinoid *Kalbarria brimmellae* that is among the earliest evidence for land inhabitation (McNamara & Trewin, 1993; Trewin & McNamara, 1995). *Skolithos*-type bioturbation indicating marginal marine environments is common in coastal outcrops of the Tumblagooda Sandstone south of Kalbarri, as are *Heimdallia* freshwater burrows that are typical of shallow pools in tidal sandflat deposits (Trewin & McNamara, 1995). Retallack (2009) reported the occurrence of calcic paleosols in the fluvial facies of the Tumblagooda Sandstone and correlated these across Australia as indicators for continent-wide paleoclimate changes.

Based on previous U–Pb zircon geochronology it was argued that sediment source regions were located to the north (Capricorn Orogen), east (Yilgarn Craton), south (Albany-Fraser Orogen; Mawson Orogen), and from the underlying Pinjarra Orogen (Byrne, 1997; Bruguier et al., 1999; Cawood & Nemchin, 2000; Johnson, 2013; Myers, 1995; Myers et al., 1996; Figure 10). Paleocurrent analysis in the lower Murchison River area by Mandyczewsky (1973) suggested that the Northampton Complex was not exposed during the deposition and therefore not an apparent contributor to the detrital zircon record of the Tumblagooda Sandstone.

3. Methods

3.1. U–Pb Zircon Geochronology

U–Pb zircon ages were obtained by Laser Ablation Inductively Coupled Plasma Mass Spectrometry (LA-ICP-MS) from 16 samples of the Tumblagooda Sandstone including 10 drill core samples and 6 outcrop samples, resulting in a total of 1,980 zircon spot analyses. Zircon grains were separated from crushed material using hand panning. No magnetic separation was performed to avoid bias in the detrital zircon populations induced by sample preparation. Between 120 and 150 zircon grains were randomly selected (all colors and grain shapes) and mounted in epoxy resin. Polished zircon mounts were imaged with a TESCAN VEGA3 Scanning Electron Microscope (Centre for Microscopy, Characterization and Analysis; The University of Western Australia) and ablated using the LA-ICP-MS at the John de Laeter Centre (Curtin University, Australia). Detailed descriptions and laser-specific parameters are listed as Figure S1 in the supporting information. Analyses within $\leq$10% of concordia were used for provenance investigation. All discordant data ($>$10% discordance) were used for U–Pb zircon discordance modeling after Reimink et al. (2016). This statistical method generates a "discordia likelihood map" with lower intercepts that indicate the age of potential Pb-loss events and corresponding potential crystallization ages at the upper intercept.

3.2. Whole Rock Geochemistry

Ten samples from Wendy-1 and Coburn 1 drill cores of predominantly medium- to coarse-grained sandstones were analyzed for whole-rock geochemistry in order to obtain sandstone chemical compositions and interpret the level of maturity. Sample material of the $<$2 mm fraction was subsequently milled and analyzed by the Geological Survey of Western Australia (GSWA). Whole rock samples were analyzed by

inductively-coupled plasma spectrometry using a series of in-house standards from GSWA for major oxides. The analytical data are also available under the respective sample numbers in the WACHEM database of GSWA (http://www.dmp.wa.gov.au/GeoChem-Extract-Geochemistry-1559.aspx).

3.3. Infrared Reflectance Spectroscopy

Infrared reflectance spectroscopy, used on both drill cores (Wendy-1 and Coburn 1), is a mineral analysis technique that can be used to enhance conventional core descriptions through the detection of alteration and rock-forming mineralogy (Clark et al., 1990; Hunt, 1977; Kruse, 1996). Detailed descriptions and background information of this method can be found in Figure S1.

4. Results and Interpretations

4.1. Stratigraphy and Depositional Environment

The stratigraphic succession of the Tumblagooda Sandstone is interpreted from approximately 520 m strata of the Wendy-1 and approximately 120 m strata of the Coburn 1 stratigraphic wells (Figures 2 and 3; detailed logging observations in supporting information S2 and S3). Both drill cores represent different levels in the stratigraphy. While strata in Wendy-1 were deposited unconformably on top of basement rocks of the Pinjarra Orogen in the northern Perth Basin and contain strong fluvial redbed sequences, strata in Coburn 1 include the upper boundary of this succession with a conformable transition to the Early Silurian Dirk Hartog Formation. Even though the cores contain strata of different stratigraphic levels within the Tumblagooda Sandstone, the sedimentary composition is similar.

Sediments in the basal successions of both drill cores are dominated by a monotonous succession of trough cross-beds, high- and low-angle planar cross-bedding, and laminated sand units with minor incisions of small-scale troughs. These observations are consistent with a strong alluvial succession characterized by an irregular bedding style reflecting a bed load dominant depositional regime, with high rates of sediment transport. From outcrop sections in the Murchison Gorge and coastal cliffs, it can be inferred that the successions in the cores reflect a stacked sand sheet alluvial architecture, often encountered in prevegetation alluvial successions. Sediments are coarse- to medium-grained with thin pebble layers and some prominent conglomerate horizons. The medium to coarse-grained sandstones are generally poorly sorted with a low degree of roundness of quartz and feldspar grains and bounded by Fe-oxide concentrations and rims. The overall characteristics are consistent with the general claim of a braided style of alluvial deposition (Hocking, 1987). The upper parts of both cores show a distinctively different depositional style with medium- to fine-grained massive sandstone beds. The preservation of small-scale symmetric ripples in fine-medium grained, well sorted sandstone units points to oscillatory currents. These ripple forms, associated with pervasive bioturbation structures, support a nearshore environment of deposition interpretation.

Although the general succession of a strong red bed alluvial association and intertidal depositional environment recognized by Hocking (1987) is consistent with the stratigraphy in both cores, the examined cores could not be related to Hocking (1987) facies FA1 to FA5. We attribute this to the dynamic nature of the rift basin where one would expect a high degree of spatial variability in the sedimentary facies.

4.2. Sandstone Composition and Alteration

Whole rock geochemical analyses from 10 drill core samples were used to determine sandstone composition and levels of sediment maturity (Table 1) and to understand the weathering environment of the sediments and detect possible alteration. The relationship between elemental composition, mineralogy, and rock type was classified based on the chemical classification of the "SandClass" system after Herron (1988). This scheme considers two primary parameters, the SiO_2/Al_2O_3 ratio, which distinguishes between quartz-rich sandstones and clay-rich shales versus the Fe_2O_3/K_2O ratio, which was used to distinguish lithic fragments from feldspars (Figure 4a). Drill core samples reflect the low level of maturity of the sandstones, which can be regarded as immature in composition (Figure 4b).

The SiO_2/Al_2O_3 ratio is widely used to indicate mineralogical maturity in sediments as it is sensitive to weathering, transport, and recycling processes (Pettijohn, 1974; Pettijohn et al., 1972). All samples are enriched in SiO_2 and depleted (<1 wt %) in Na_2O, CaO, and TiO_2, which can be attributed to the small amount of plagioclase in the sediment in general. Values increase when sediments contain preferably more quartz over less

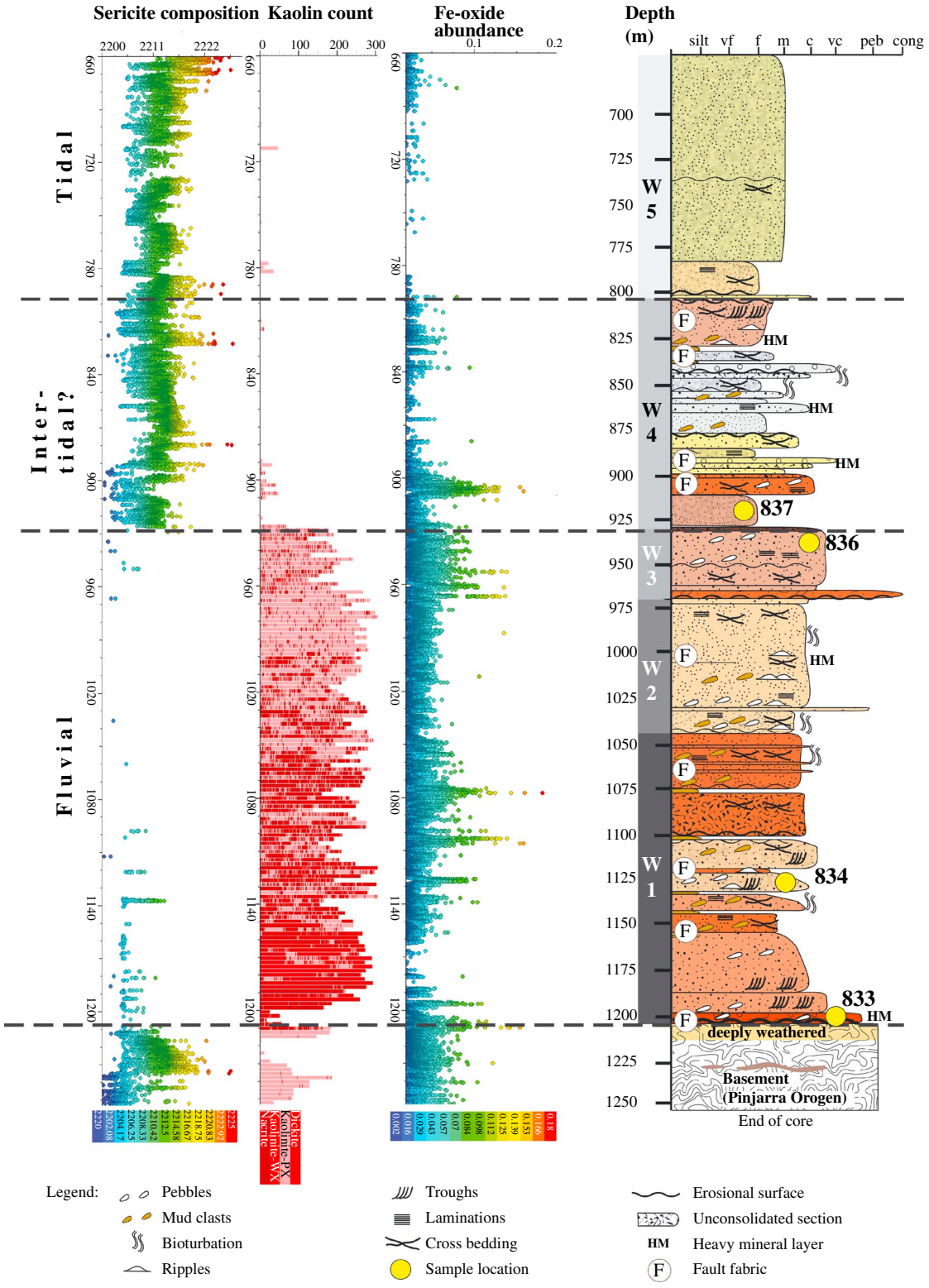

Figure 2. Spectral mineralogy and generalized sediment log of drill core Wendy-1. Results of the infrared reflectance spectroscopy are shown as color-coded scatterplots, where the *y* axes correspond to core depth (m), and the specific absorption feature depths (wavelengths in nm) and different spectral parameters are plotted on the *x* axis: (1) color-coded sericite composition, where muscovites are plotted in blue and phengites in red; (2) kaolin counts, which represent the number of kaolin samples per interval (counts); and (3) Fe-oxide abundance, which is a measure of intensity of the ferrous iron absorption feature. Kaolinite-PX (poorly ordered) and kaolinite-WX (well-ordered). The sediment log displays the five major lithofacies intervals (W1 to W5; see supporting information for detailed sedimentary descriptions); beds show the general color trend in the sediments.

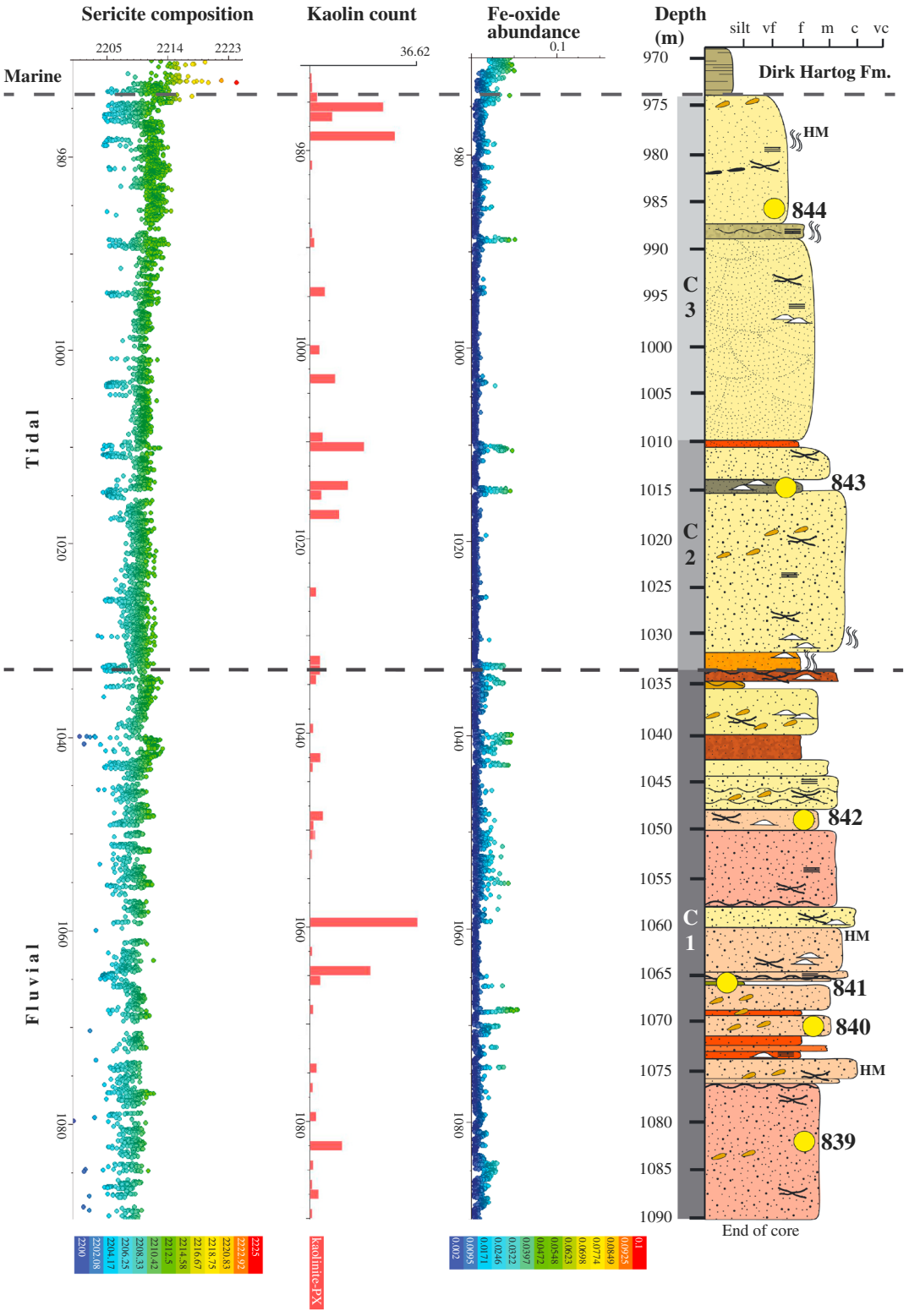

Figure 3. Spectral mineralogy and generalized sediment log of drill core Coburn 1. Results of the infrared reflectance spectroscopy are shown as color-coded scatterplots where the *y* axes correspond to core depth (m) and the specific absorption feature depths (wavelengths in nm) and different spectral parameters are plotted on the *x* axis: (1) color-coded sericite composition, where muscovites are plotted in blue and phengites in red; (2) kaolin counts, which represent the number of kaolin samples per interval (counts); and (3) Fe-oxide abundance, which is a measure of intensity of the ferrous iron absorption feature. See Figure 2 for legend. The sediment log contains the three major lithofacies intervals (C1 to C3; see supporting information for detailed sedimentary descriptions); beds show the general color trend in the sediments.

Table 1
Sandstone Classification Results, Selected Whole-Rock Geochemical Content of Major Elements, and Chemical Index of Alteration (CIA)

Sample ID	Core Depth (m)	Rock Type	Al2O3 (%)	CaO (%)	Fe2O3 (%)	K2O (%)	MgO (%)	Na2O (%)	SiO2 (%)	TiO2 (%)	Zr (ppm)	CIA
833	1,209.72–1,209.0	Sublitharenite	3.37	0.03	2.05	1.9	0.22	0.09	91.49	0.22	146	62.5
834	1,134.4–1,133.9	Subarkose	2.63	0.01	1.08	2.01	0.03	0.09	93.56	0.06	126	55.5
836	932.15–931.75	Subarkose	2.64	0.01	1.09	2.02	0.03	0.09	93.8	0.06	74	55.5
837	915.2–915.0	Subarkose	2.56	–	0.91	1.93	0.06	0.16	93.87	0.16	611	–
839	1,082.0–1,082.3	Subarkose	3.8	0.02	0.48	2.9	0.08	0.18	92.35	0.12	314	55.1
840	1,072.0–1,071.7	Subarkose	3.23	0.01	0.5	2.54	0.05	0.17	92.9	0.1	239	54.3
841	1,065.8–1,066.0	Greywacke	18.23	0.07	3.2	11.13	1.08	0.41	62.24	0.82	776	61.1
842	1,048.5–1,048.8	Subarkose	6.19	0.03	0.52	4.81	0.12	0.25	86.8	0.37	710	54.9
843	1,014.7–1,015.0	Arkose	15.35	0.06	1.7	10.93	0.62	0.32	70.08	0.33	212	57.6
844	985.8–986.1	Subarkose	3.8	0.02	0.4	3.04	0.05	0.15	92.03	0.13	320	54.2

resistant feldspars, mafic minerals, and lithic fragments (Roser et al., 1996; Roser & Korsch, 1986). The SiO_2 content in the samples ranges from 62 to 93 wt %, typical for immature sandstones such as sublitharenite, subarkose, and arkose (Figures 4a and 4b). Two samples from Coburn 1 (841 and 843) stand out from all other sandstones by displaying lower levels of chemical maturity due to increased clay content. K-feldspars dominate over plagioclase with K_2O/Na_2O ratios ≫1.

The effect of source rock weathering can be characterized by the widely used Chemical Index of Alteration (CIA) proposed by Nesbitt and Young (1982). All samples show very low CIA values between 54 and 62 with an average of 56.7 ± 1.02 (Table 1), indicating low levels of maturity in the sediments, which is consistent with their observed mineralogy (Figure 4a) and low degrees of weathering at the source.

4.3. Spectral Trends and Compositional Changes

Mineralogical trends, changes in composition, and sediment alteration were investigated using infrared reflectance spectroscopy. The most significant mineralogical spectral trends were recognized in the white mica composition, distinguishing high-Al muscovites from low-Al phengite, and the abundance of Fe-oxide and kaolin. Results were presented as color-coded plots in Figure 2 (Wendy-1) and Figure 3 (Coburn 1), whereas detailed descriptions can be found in supporting information S4.

Although the lithological variation in the sediments of the Tumblagooda Sandstone is only minor, infrared reflectance spectroscopy identified major mineralogical shifts within this succession. The main mineral assemblages in the sandstone units contain mostly quartz with variable feldspar and either dominating sericite ± chlorite or kaolinite and Fe-oxide in the matrix. The mica composition varies in a systematic manner between muscovite (high-Al/low Si) and phengite (low-Al/high Si), reflecting the formation of distinct potassium alteration (Figure 2). The occurrence of various types of sericite is primarily due to lithological variations, where phengite occurs in finer grained sandstone and siltstone beds, and muscovite and phengitic muscovite is associated with medium- to coarse-grained sandstone beds. With the occurrence of sericite in sediments of Wendy-1 at 926 m, Fe-oxide contents decrease rapidly. In sandstone sequences depleted in sericite, kaolinite is the dominant mineral phase, accompanied by abundant Fe-oxide, which defines a typical red bed facies. The change in clay mineralogy represents either a change in source material, alteration of sediments during burial diagenesis, or a change in depositional environment. It is noteworthy that the distinct shift from kaolinite to sericite occurs in association with changes in sediment

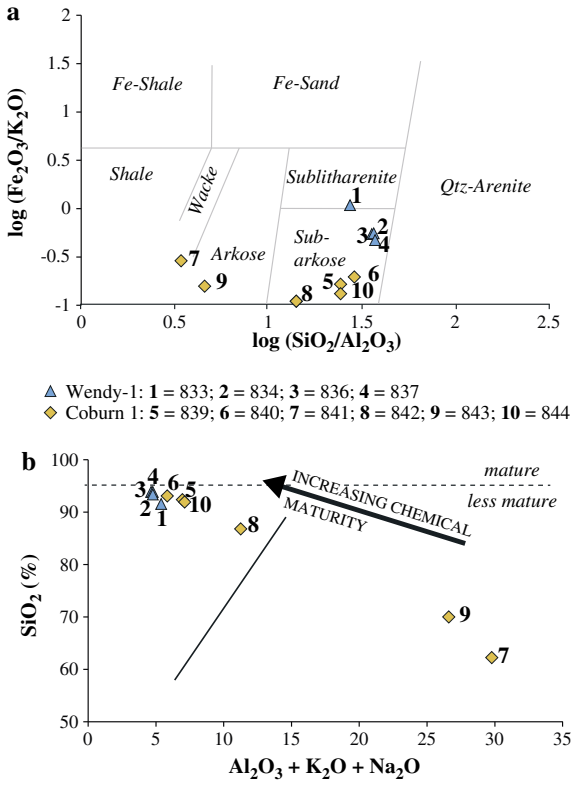

Figure 4. Chemical classification system for Tumblagooda Sandstone drill core samples (Wendy-1 and Coburn 1) from the northern Perth and Southern Carnarvon basins (after Herron, 1988): (a) relationship between elemental composition, mineralogy, and rock type; (b) maturity levels in sediments.

characteristics and bedding styles. Consequently, we interpret this kaolinite-sericite change as marking the transition from the basal alluvial succession to a near-shore tidal depositional setting.

4.4. Detrital Zircon U–Pb Geochronology and Age of Tumblagooda Sandstone

We acquired a total of 1,945 U–Pb analyses, including 737 concordant ages (≤10% discordance) from 16 Tumblagooda Sandstone samples, including 10 drill core samples (four samples from Wendy-1: 833, 834, 836, and 837; total of 169 concordant ages and 6 samples from Coburn 1: 839 to 844; total of 212 concordant ages). Six outcrop samples were collected (822, 821, 818, 825, and 827; total of 356 concordant ages) representing the type sections FA1 to FA4 (Hocking, 1987). The LA-ICP-MS U–Pb zircon data are given in the table of supporting information S5. All analyses are shown on inverse concordia diagrams (Figure 5).

Detrital zircon grains are typically subhedral with elongated to stubby habits; the edges are rounded and the grain surfaces pitted. Grains occur as fragments as well as pristine needle-like grains. While there is a high variability of grain sizes for the entire data set, the largest zircon grain has a length of 397 μm and a width of 172 μm (upper section of Wendy-1: 837). The smallest grain has a length and width of 5.9 μm (upper section of Coburn 1: 841). Archean zircon grains are on average smaller in width and length than Proterozoic and Paleozoic grains (e.g., the mean length is 141 μm for Archean grains, 164 μm for Proterozoic, and 176 μm for Paleozoic grains). Grain width averages show the same trend with smaller widths in Archean grains (85 μm) compared to Proterozoic (89 μm) and Paleozoic (92 μm) grains, although differences in width are more subtle than in length (Table 3 and supporting information S5). Archean grains have smaller length to width ratios (1:1.6) compared to Proterozoic (1:1.8) and Paleozoic (1:1.9) grains, which may result from a more prolonged duration of abrasion and erosion on the grain's surfaces (e.g., Markwitz & Kirkland, 2017; Shaanan & Rosenbaum, 2016). Significantly, the Archean zircon population in sample 833, which is located at the base of the sequence, is on average 5% larger than the Archean population in upper stratigraphic levels.

Zircons are characterized by either well-developed oscillatory zoning (interpreted to indicate a magmatic origin) or featureless, irregular internal structures (interpreted to indicate recrystallization or a metamorphic origin (e.g., Taylor et al., 2016; Vavra et al., 1996). In cathodoluminescence (CL) images the internal textures of Archean grains are predominantly irregular and featureless, with bright rims, and a minority of grains (843 and 844) showing well-defined oscillatory zonation. In contrast, most Proterozoic zircon grains display faint to intense oscillatory zonation and only a few grains show irregular and featureless internal textures. Some Proterozoic grains have homogeneous rims that indicate metamorphic overgrowth in the source rocks. The youngest age group in the detrital population of the Tumblagooda Sandstone consists exclusively of finely zoned zircons interpreted to reflect an igneous genesis. CL images of representative detrital zircon grains are shown in Figures 6a–6j. The calculated ages of all samples are presented as stacked probability density plots to display variations in zircon provenance in stratigraphic order for both drill cores and by facies associations (FA 1 to FA 4) for the outcrop samples (Figure 7 and Table 2).

4.4.1. Maximum Age Constraint for Deposition

Provenance interpretation is based exclusively on concordant zircon ages (≤10% discordance). The youngest detrital zircon grain of 737 concordant analyses within the Tumblagooda Sandstone provides a maximum depositional age constraint of 466 ± 8 Ma (sample 841; Coburn 1). A more conservative estimate of the maximum age of deposition is provided by calculating the weighted mean of 481 ± 3.5 Ma (mean square of weighted deviates = 1.01) from the five youngest ages.

U concentrations for the youngest detrital zircon grains are relatively low, ranging from 31 to 642 ppm. The calculated apparent density (after Murakami et al., 1991) for the youngest age group ranges from 4.70 to 4.75 g/cm^3, indicating a crystalline structure. Across all samples, the youngest single grain can be ascribed to an original magmatic population that has not lost radiogenic Pb. The youngest age of 466 ± 8 Ma from Coburn 1 (sample 841; 1,065.8–1,066 m) drill core is within uncertainty of the youngest age of 468 ± 11 Ma reported in Wingate et al. (2015) from the Rainbow Valley coastal outcrop.

4.4.2. Sample Similarities and Potential Provenance

The Kolmogorov-Smirnoff (K-S) test compares age distributions between individual samples and tests the probability if the populations were derived from a common source (Birnbaum, 1952; Drew et al., 2000; Sircombe & Hazelton, 2004). Based on the K-S test a multidimensional scaling diagram (MDS) has been constructed as a means to graphically interpret the statistically based detrital similarity comparison (Figure 8;

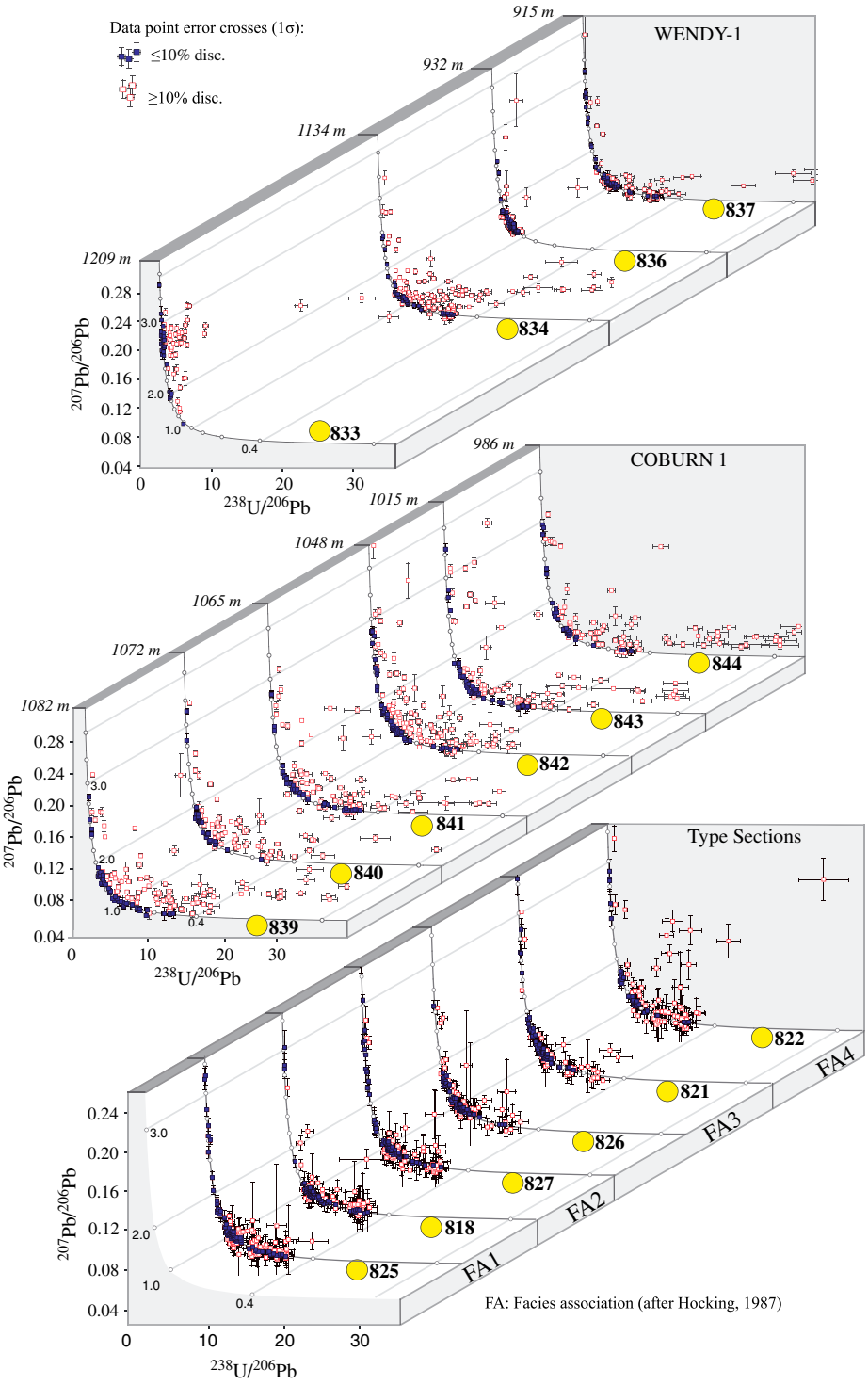

Figure 5. Stacked inverse concordia diagrams for Tumblagooda Sandstone samples for Wendy-1 and Coburn 1 drill cores and also samples from the Murchison Gorge in order of facies associations (after Hocking, 1987).

Vermeesch, 2013; Spencer & Kirkland, 2016; Vermeesch et al., 2016). This diagram was generated using the "provenance" package in R (Vermeesch et al., 2016). In the diagram the pairwise distances between similar U–Pb age distributions are plotted to be directly proportional to the dissimilarities between corresponding samples. The MDS diagram shows that most of the samples cluster, indicating similar U–Pb age distributions, except for sample 833 (basal sequence of Wendy-1; 1,209.72–1,209 m), 836 (Wendy-1;

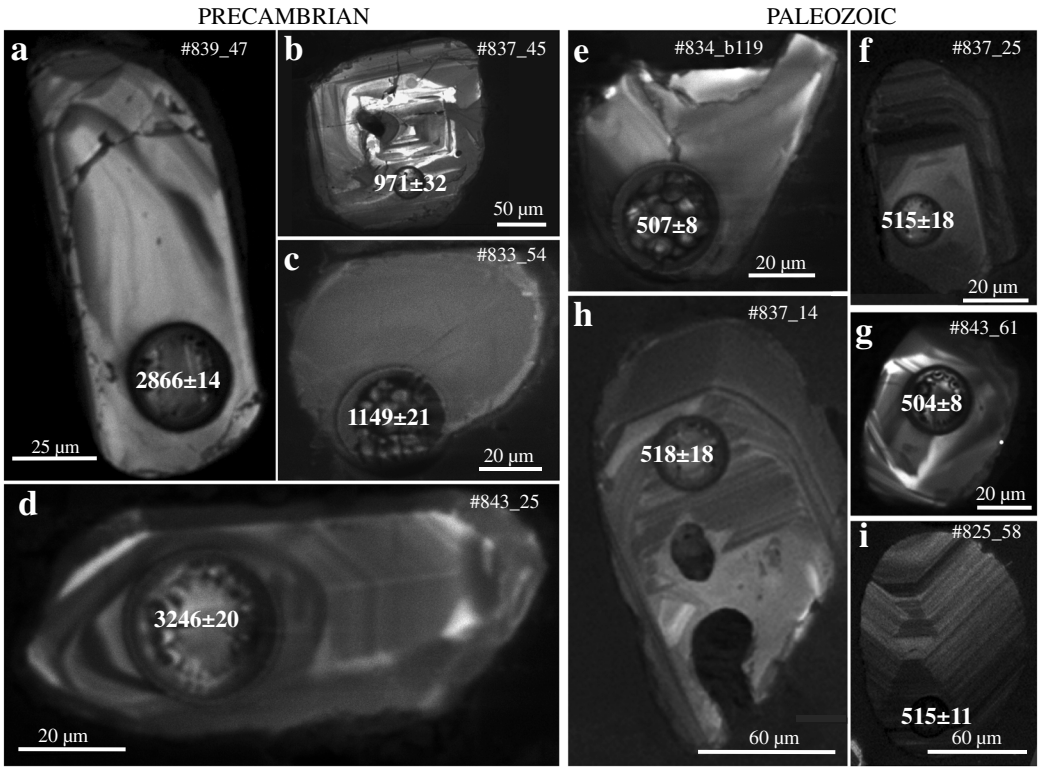

Figure 6. Cathodoluminescence images of selected detrital zircons highlighting location of laser spot, U–Pb age, and short sample number along with grain spot number. Precambrian zircon internal structures are interpreted to reflect both (a and c) metamorphic genesis and (b and d) igneous. (e–i) Typical Paleozoic igneous zircon grains are presented.

932.15–931.75 m), and possibly 818 (type section; Murchison Gorge), which scatter along vectors toward greater incorporation of Archean (2.8–2.7 Ga; 833), Mesoproterozoic (1.7–1.2 Ga Ma; 836), and Neoproterozoic (1.12 Ga; 818) age components. The latter samples therefore reflect more distinct zircon age spectra.

4.4.3. U–Pb Discordance Modeling

Approximately 60% of U–Pb zircon analyses are discordant (>10% discordance). This, to some extent, is a function of the sample preparation and grain selection procedure employed, as no magnetic separation was performed and grains were selected unsystematically (irrespective of coloration, shape, or appearance) to avoid sampling bias and to retain a representation of all material present. Highly discordant analyses are most common in Archean grains with higher U contents (>500 ppm), consistent with enhanced radiogenic-Pb loss due to metamictization. U–Pb discordance modeling (Reimink et al., 2016) allows important information to be extracted from discordant analyses. Based on discordance modeling, major detrital age peaks are found at 2,828 Ma, 2,388 Ma, and 1,763 Ma with corresponding lower intercept ages at 89 Ma, 85 Ma, and 470 Ma implying major Pb-loss events in the Ordovician and Late Cretaceous (supporting information S6a). However, when the U–Pb disturbance model produces a major peak, for example, at 1,240 Ma (see supporting information S6a) with no corresponding lower intercept peak, no meaningful Pb loss event can be determined. In the discordia likelihood map (supporting information S6b), major Pb loss events at ~470 Ma and ~85 Ma to 89 Ma are indicated.

5. Discussion

U–Pb zircon geochronology on systematically sampled stratigraphic levels coupled with infrared spectroscopy and field and drill core lithological observations allow us to characterize the depositional environment of the Tumblagooda Sandstone and provide a robust maximum age for deposition.

The relative mineralogical immaturity of the sandstones, particularly within the medium- and coarse-grained beds, is typical for prevegetation terrestrial environments (Went, 2013). The sandstones are principally

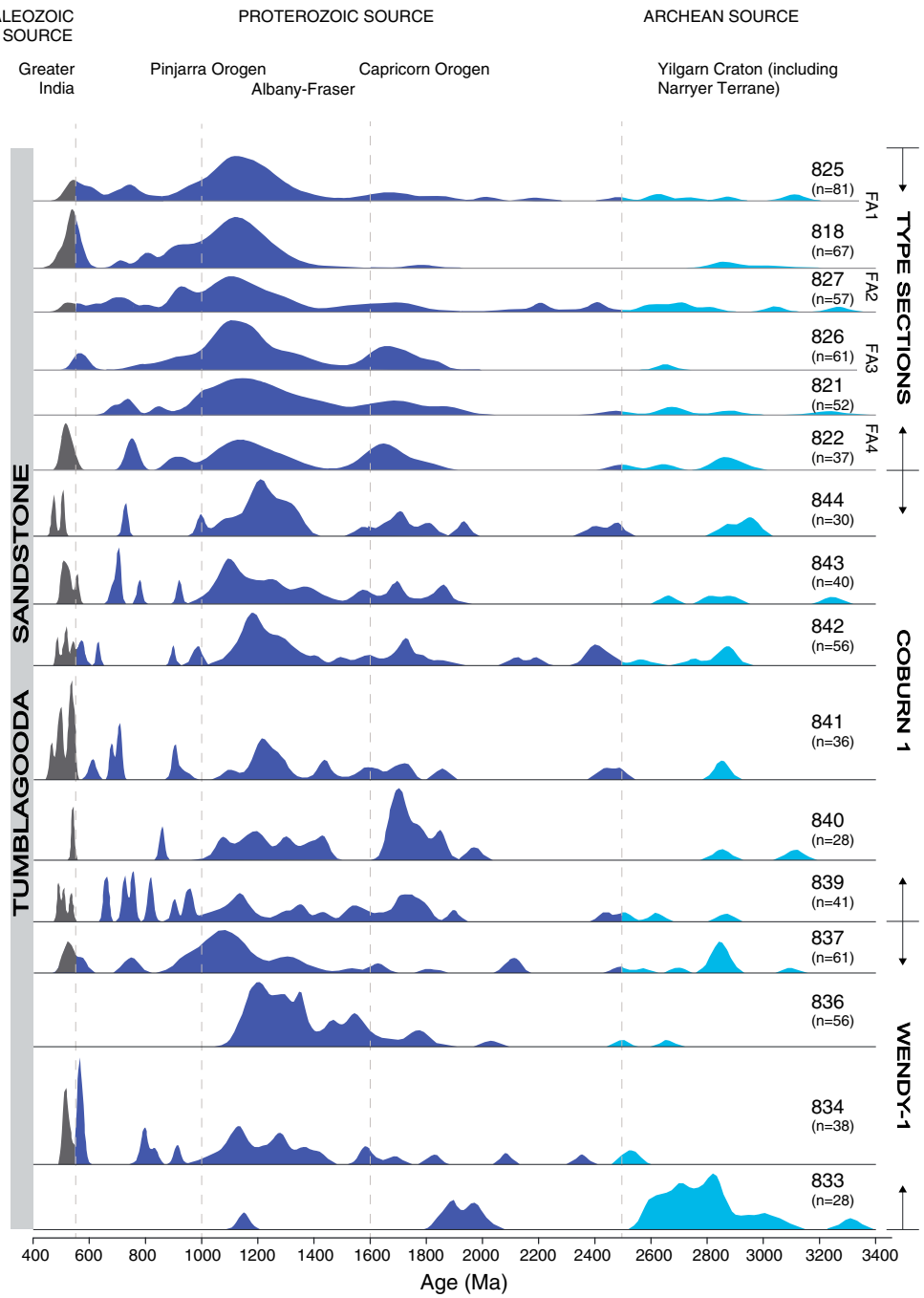

Figure 7. U–Pb detrital zircon age spectra displayed in normalized probability density plots ($n \leq 10\%$ discordant ages) of the Tumblagooda Sandstone from all drill core samples (Wendy-1 and Coburn 1) and outcrops from the Murchison Gorge and coastal cliffs. Three major source regions are outlined: (1) "Archean" zircon provenance in light blue, (2) "Proterozoic" provenance in blue, and (3) "Early Paleozoic" provenance in dark gray.

subarkosic to arkosic in composition with a high proportion of quartz and significant amounts of K-feldspar over the more chemically unstable plagioclase, suggesting dynamic erosion of an exposed proximal granitic or metamorphic source. Low CIA values support low maturity levels (Table 1 and Figure 4) and indicate low degrees of weathering at the source, with large amounts of feldspar-rich detritus eroded from the hinterland and rapidly deposited with incomplete reworking. Even though the general composition of sandstone units did not change dramatically through the stratigraphic section in the drill cores, an important compositional boundary at 926 m core depth in Wendy-1 was identified by infrared spectroscopy (Figure 2). At this boundary, the change in bedding style is clear and illustrates the transition from strong fluvial to intertidal

AGU Tectonics

10.1002/2017TC004696

Table 2
Summary of U–Pb Zircon Age Results, Including Sample Locations, Major Age Peaks, and Oldest and Youngest Grain Age for Each Age Spectra

ID	Core Depth (m)	Lat/Long	Location	Total Number of Analyses/ Concordant Ages	Main Age Peaks (Ma; Number of Analyses)	Oldest Age (Ma)	Youngest Age (Ma)
Coburn 1							
844	985.8–986.1	−26.699/ 114.226	Southern Carnarvon Basin	118/30	1,706 (3); 1,208 (9)	2,972 ± 24	472 ± 8
843	1,014.7–1,015			141/40	1,860 (3); 1,695 (3); 1,368 (5); 1,247 (7); 1,096 (10); 704 (3)	3,246 ± 20	504 ± 8
842	1,048.5–1,048.8			172/56	2,879 (3); 2,403 (4); 1,731 (5); 1,181 (15)	2,881 ± 11	485 ± 6
841	1,065.8–1,066			158/36	1,431 (3); 1,262 (7); 1,218 (6); 535 (3); 499 (3)	2,856 ± 19	466 ± 8
840	1,072–1,071.7			96/28	1,849 (3); 1,701 (7); 1,429 (3); 1,190 (5); 1,075 (3)	3,115 ± 12	541 ± 4
839	1,082–1,082.3			150/41	1,744 (4); 1,708 (4); 1,544 (3); 1,135 (7); 943 (4)	2,866 ± 44	490 ± 6
Type Sections							
FA1							
825	N/A	−27.875/ 114.559	Hardabut Fault	151/81	541 (5); 741 (5); 1,122 (42); 1,673 (6); 1,832 (3)	3,122 ± 32	513 ± 19
818		−27.788/ 114.467	Hawks Head	123/67	538 (9); 806 (4); 1,122 (39)	3,017 ± 61	486 ± 21
FA2							
827		−27.654/ 114.458	Z-Bend	112/57	703 (4); 928 (13); 1,104 (23); 1,691 (6); 2,206 (3); 2,408 (3)	3,270 ± 22	515 ± 20
FA3							
826		−27.544/ 114.433	Top-Loop (West Lookout)	108/61	564 (3); 1,108 (30); 1,658 (11)	2,653 ± 29	549 ± 18
821		−27.745/ 114.139	Red Bluff	90/52	1,143 (25); 1,693 (7); 1,860 (3)	3,235 ± 52	686 ± 21
FA4							
822		−27.757/ 114.137	Rainbow Valley	95/37	514 (4); 750 (3); 1,136 (12); 1,647 (8)	2,925 ± 46	506 ± 14
Wendy-1							
837	915.2–915	−28.309/ 115.016	Northern Perth Basin	131/61	2,841 (7); 1,303 (8); 1,079 (19); 748 (3); 523 (4)	3,100 ± 14	515 ± 18
836	932.15–931.75			83/56	1,770 (4); 1,543 (9); 1,465 (7); 1,348 (13); 1,286 (16); 1,202 (15)	2,659 ± 12	1,147 ± 25
834	1,134.4–1,133.9			160/38	1,364 (3); 1,277 (5); 1,130 (6); 565 (5); 515 (4)	2,547 ± 15	507 ± 8
833	1,209.72–1,209			48/28	2,826 (7); 2,771 (4); 2,640 (3); 1,968 (3); 1,893 (3)	3,312 ± 11	1,149 ± 21

Table 3
Grain Size Statistics of Concordant Detrital Zircon Age Populations in the Tumblagooda Sandstone, Sorted According to Their Age

	Archean			Proterozoic			Paleozoic		
	Length (μm)	Width (μm)	*n*	Length (μm)	Width (μm)	*n*	Length (μm)	Width (μm)	*n*
Coburn 1									
Range	86–180	45–101	17	61–288	46–119	156	89–222	43–105	14
Mean	121	71		130	74		141	77	
Median	119	70		124	73		139	78	
STD	32	16		42	16		41	17	
Type Sections									
Range	129–277	74–187	24	104–449	58–245	276	147–287	62–165	11
Mean	201	112		202	107		233	123	
Median	204	107		193	100		239	121	
STD	53	30		60	29		44	33	
Wendy-1									
Range	86–242	56–165	27	64–275	38–131	113	106–207	49–124	4
Mean	140	86		134	81		171	91	
Median	137	81		131	81		186	96	
STD	36	21		37	18		45	31	
All Samples: *Tumblagooda Sandstone*									
Range	68–277	57–187	67	61–449	38–245	545	89–287	43–165	29
Mean	141	85		164	89		176	92	
Median	136	81		151	86		176	89	
STD	33	19		56	24		55	30	

Note. *n* = number of concordant analyses (≤10% disk); STD = standard deviation.

depositional environments. This change cannot be correlated to the facies associations (FAs) reported by Hocking (1987).

5.1. Denudation of the Yilgarn Craton in the Early Paleozoic and Basin Evolution

Concordant age data from a large number of samples highlight the differences of preserved age spectra in the succession (Figure 7). Most of the samples contain similar zircon age spectra that span from Early Paleozoic to Archean populations, indicating derivation from mixed cratonic sources. However, samples 833 and 836 (Wendy-1) and also sample 818 (outcrop in Murchison Gorge) yield significantly different age fractions (see also section 4.4): sample 833 contains dominantly Archean, 836 dominantly Mesoproterozoic, and 818 dominantly Neo-Mesoproterozoic ages in contrast to the rest of the samples. Dominantly Archean ages in sample 833 reflect a scarcity of multiple recycled material and highlight that input was likely from a singular primary source. Samples displaying a wide range of ages most likely contain multiply recycled sediments. In Sample 833, 75% of the total detrital zircon population is Archean, implying that deposition on the basement rocks of the Northampton Complex coincided with denudation and erosion of the Yilgarn Craton. This in turn suggests that part of the Yilgarn Craton was exposed and available as a source during the Early Paleozoic rather than being covered by Proterozoic and Paleozoic strata (cf. Cawood & Nemchin, 2000). If the Yilgarn Craton had been covered at the time of Tumblagooda Sandstone deposition, the majority of detrital zircon age components, particularly in the basal section, should contain multicycle material that would have been sourced from sedimentary rocks that themselves lack any Proterozoic and Paleozoic components. As no such rock unit is known, this scenario is considered unlikely.

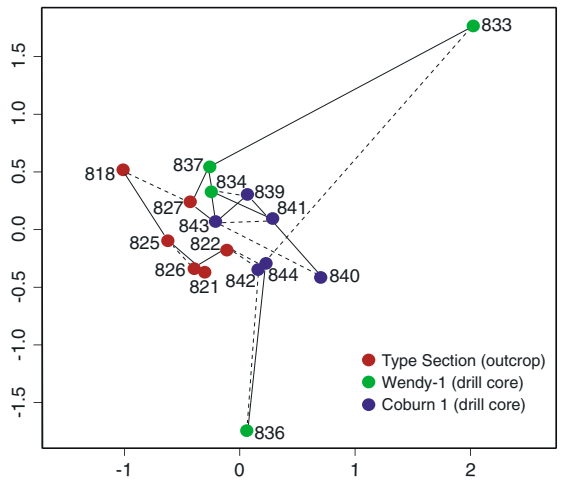

Figure 8. Multidimensional scaling diagram of directly proportional dissimilarities between corresponding samples (after Vermeesch, 2013; Vermeesch et al., 2016). The solid lines correspond to the closest neighbor and the dashed lines the second closest neighbor. Samples are color-coded for better identification of drill core and outcrop samples.

The 470 Ma age calculated by U–Pb disturbance modeling highlights a distinct Pb loss event in the Archean zircon population from Yilgarn Craton rocks. Similar ages are known from Rb-Sr ages as young as

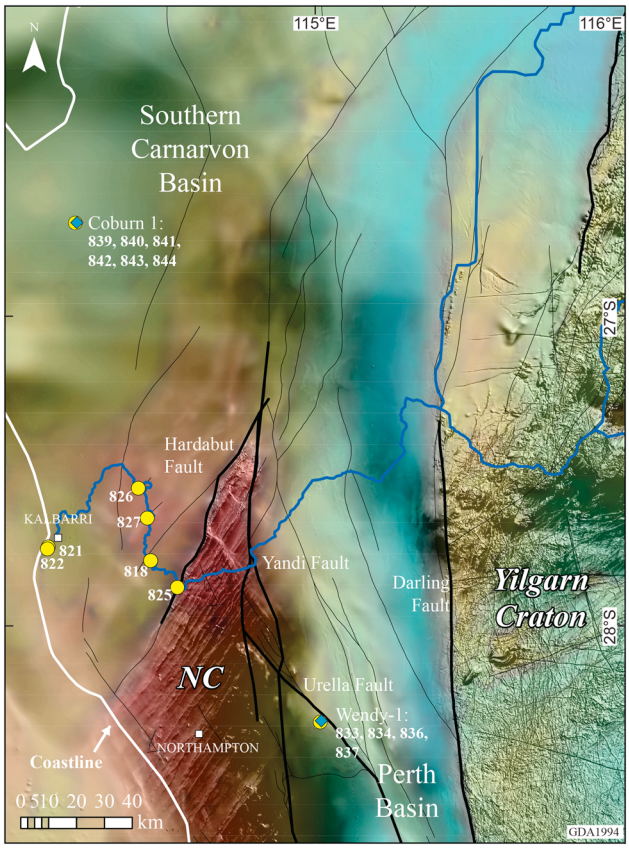

Figure 9. Combined gravity (color) and magnetic anomaly map (shading) illustrates the highly segmented basement of the Pinjarra Orogen (red colors), the proximity to the Archean Yilgarn Craton, and depth structure of basins (blue colors; NC, Northampton Complex; the yellow points represent sample locations; the yellow points with blue squares represent drill core locations).

~430 Ma in the western Yilgarn Craton (Libby et al., 1999) and from zircon Raman radiation damage ages of an Archean Darling Range granite (420 ± 110 Ma; Pidgeon, 2014). Although a considerable distance to the western margin of the Yilgarn Craton, zircon Raman radiation damage ages of ~500 Ma have also been reported from an East Pilbara Archean gneiss (Wiemer et al., 2017). The Pb loss at 470 Ma occurred exclusively in the Archean zircon population and occurred within error of the age of the youngest detrital zircon (466 ± 8 Ma). This implies that the Pb loss event either occurred in the Archean source rock or during early diagenesis in the basin. Our preferred interpretation is to relate the 470 Ma U–Pb disturbance age to leaching of radiogenic Pb by surface fluids during denudation and uplift of the western Yilgarn Craton, because there is no evidence of a Pb loss event in the Proterozoic age population. This age therefore provides another independent constraint for the minimum sediment age and therefore the maximum depositional age of the Tumblagooda Sandstone. U–Pb disturbance modeling also highlights a Late Cretaceous Pb loss alteration event (supporting information S6), which would have occurred in the basin after the Jurassic breakup of Greater India and Australia but, at present, cannot be linked to any specific known regional thermal or fluid-flow event in the Southern Carnarvon Basin or northern Perth Basin.

5.2. Basement Segmentation of the Pinjarra Orogen and Basin Architecture

The Pinjarra Orogen was segmented during Mesozoic rifting and the opening of the Indian Ocean, which caused reactivation of the Darling and Urella Faults (Figure 9; Janssen et al., 2003; Hall et al., 2013). A combined gravity and magnetic map of the study area highlights the segmentation, thickness of the basins, and significance of regional large-scale structures. The lowest succession of the Tumblagooda Sandstone displayed in Wendy-1 drill core contains very coarse sandstone and conglomerates that rest on the eastern part of the Northampton Complex basement shoulder and have dominantly Paleo- to Mesoarchean zircon ages (sample 833), interpreted to be sourced from the Yilgarn Craton. In contrast, the strata represented in the Murchison Gorge type section near the Hardabut Fault (Figure 1) rest on the western part of the topographic high of the Pinjarra Orogen (Northampton Complex) but display a complex zircon provenance yielding Paleozoic to Paleoarchean zircon ages (486 Ma–3,270 Ma; Table 2). The type section outcrops in the Murchison Gorge and along coastal cliffs, located west of the Yandi Fault and Hardabut Fault, most likely represent a different part of the basin, underlain by different basement units of the Pinjarra Orogen (Figure 9). Given the segmentation of the Pinjarra Orogen basement, it is possible that elements of the present-day architecture, such as the relatively elevated position of the Northampton Complex, already existed during basin formation. For this to be the case, a significant difference in basin fill (e.g., variations in zircon age spectra) would be expected on either side of the Northampton Complex. This seems to be the case, at least for the basal units represented in Wendy-1 and at the Hardabut Fault location, because sample 833 at the base of Wendy-1 yields Archean-dominated zircon ages and sample 825 from outcrop near the Hardabut Fault contains Paleozoic to Archean aged zircon grains (Figure 7). The youngest single grain age reported from the Tumblagooda Sandstone (466 ± 8 Ma) was obtained from a sample located west of the Northampton Complex (Coburn 1: sample 841; Figure 1). Also, the MDS diagram illustrates similarities in the source regions between Coburn 1 samples and type section samples, all of which are located west of the Northampton Complex (Figure 8). In contrast, the only known Archean-dominated sample was found to the east of the Northampton Complex at the base of Wendy-1, where the youngest detrital zircon also has a somewhat older age of 507 ± 8 Ma (sample 834; Table 2). Cawood and Nemchin (2000) reported a youngest detrital grain age of 474 ± 8 Ma from an outcrop sample located on the eastern part of the Northampton Complex. Their sample likely represents a higher stratigraphic level compared to

Figure 10. Paleogeographic reconstruction map showing parts of East Gondwana and location of study area (black box). The Tumblagooda Sandstone zircon provenance from mixed cratonic source regions are recognized from the West Australian craton (mainland Australia; AFO, Albany Fraser Orogen; PJO, Pinjarra Orogen) and Greater India, highlighted as red arrows.

Wendy-1 samples. MDS results also display that source similarities in the Tumblagooda Sandstone become stronger up section. It therefore seems likely that the present-day Northampton Complex constituted a basement high during the onset of sedimentation and that separate subbasins formed on either side and likely became one single basin as subsidence progressed. These observations are supported by the grain size differences within the Archean age fraction, highlighting larger Archean detrital zircons in the basal section of the Tumblagooda Sandstone (sample 833) compared to upper section Archean fractions. The number of Archean zircons within higher stratigraphic levels of the Paleozoic Tumblagooda Sandstone is therefore plausibly reduced due to prolonged duration of abrasion of the grain's surfaces during multiple recycling. In summary, the lower stratigraphic levels within this succession yield distinct age spectra, incomparable to those further up the stratigraphy. Samples located higher in the stratigraphy become more similar across the basin (MDS diagram; Figure 8).

5.3. Zircon Provenance Variations in the Tumblagooda Sandstone

The study identifies mixed cratonic sources with considerable differences in zircon provenance between samples. Analyzing samples in stratigraphic order has allowed us to identify unique changes in zircon age spectra, from samples containing dominantly Archean (833), Mesoproterozoic (836), or Neo-Mesoproterozoic (818) ages. Furthermore, samples 833 and 836 (Wendy-1) and 821 (Red Bluff; south of Kalbarri) show a lack of Early Paleozoic ages to all other samples, which yield the full range between Paleoarchean and Early Paleozoic ages. This study identified two major detrital zircon provenances, a dominant Precambrian source and a distinct Paleozoic source (Table 2 and Figure 7):

1. Precambrian sources are represented by Paleoarchean to Neoproterozoic ages (3,312 Ma to 3,739 Ma). Archean sources derived from continental granitic source rocks of the northern Yilgarn Craton, including the Narryer Terrane (Kinny et al., 1988, 1990), with ages clustering between 2,586 Ma and 3,312 Ma (Figure 7). The Paleoproterozoic age components were apparently derived from the Capricorn Orogen (Libby et al., 1986; Sheppard et al., 2007) with typical ages peaking around 1,893 Ma. With an abundance of late Mesoproterozoic (1,023–1,316 Ma) and fewer Neoproterozoic (750–943 Ma) age components, source regions contributing to the detritus in the Tumblagooda Sandstone could also be the Pinjarra Orogen itself (Bruguier et al., 1999) and the Albany-Fraser Orogen (Spaggiari et al., 2015; Figure 10). The high variance in the distribution of age clusters in the sediments suggests complex drainage network arrangements across a variety of exposed basement areas during deposition. Notably, the deposition of larger, dominantly Archean zircon grains at the base of Wendy-1 implies parts of both; the Northampton Complex and Yilgarn Craton were exposed at the same time during Paleozoic rifting. The Northampton Complex represented a topographic basement high separating subbasins and the Yilgarn Craton a proximal source for the large Archean zircon grains.
2. The Paleozoic source region is defined by the occurrence of Cambrian-Ordovician magmatic zircon ages (466 Ma to 540 Ma), which were present in 13 samples out of 16 (Figure 7). The abundance of these exclusively igneous ages puts earlier speculations of a Greater India link on a more solid base. We suggest that this age group included significant contributions from the North Indian Orogen, which, according to the relatively immature nature of the sediment, would have been located close to the Southern Carnarvon Basin (Bhimphedian Orogeny at 470–550 Ma; e.g., Cawood et al., 2007; Wang et al., 2010; Figure 10). Although the East Antarctic Orogen was proposed as a source region for Paleozoic age clusters by Cawood and Nemchin (2000), the low level of sediment maturity suggests shorter transport distances. While metamorphic Cambrian ages are known from the Pinjarra Orogen (Leeuwin Complex: Collins, 2003; Wendy-1 basement: Markwitz et al., 2017), it can be ruled out as possible source regions for detrital zircons in the Tumblagooda Sandstone because the youngest detrital zircons are magmatic in origin.

The maximum age of deposition is constrained to be less than the age of the youngest detrital zircon. The Tumblagooda Sandstone, including the trackways of terrestrial arthropods, must therefore be younger

than 466 Ma (Middle Ordovician-Darriwilian). An accurate minimum age constrain for the Tumblagooda Sandstone cannot be estimated by isotopic age measurement due to the lack of volcanic marker horizons, younger cross cutting intrusives, or diagenetic phosphate minerals, although the uppermost strata of Wendy-1, which are of questionable relation to the Tumblagooda Sandstone, contain Early Devonian fish scales (Allen & Trinajstic, 2017).

6. Conclusion

The Tumblagooda Sandstone yields detrital zircon age spectra ranging from Paleoarchean to Early Paleozoic. Out of the 16 samples, only 833, 836, and 818 are unique in their dominance of Archean (833), Mesoproterozoic (836), and Neo-Mesoproterozoic (818) age populations and their lack of Early Paleozoic ages (sample 833 and 836). These samples reflect less recycled material within the succession and may better represent a singular source region. Following the Kuunga Orogeny, the formation of the Tumblagooda Sandstone began with dominantly Archean detritus deposited into a rift basin that formed on variably exposed basement segments of the Pinjarra Orogen. The distribution of age spectra and provenance correlations based on K-S statistics and MDS diagram are consistent with the present-day Northampton Complex having constituted a basement high during the onset of rifting, with separate subbasins forming on either side. The Tumblagooda Sandstone has a low maturity level, suggesting that in addition to the Pinjarra Orogen (Proterozoic sources), the Western Australian Craton (Paleoarchean to Neoproterozoic sources) and Greater India (Early Paleozoic sources) were proximal and exposed during Early Paleozoic rifting in East Gondwana, possibly as rift shoulders. Our maximum age of deposition (466 ± 8 Ma) implies that the terrestrial animal activity in the Tumblagooda Sandstone—the earliest known on Earth—is younger than the Middle Ordovician. Discordance modeling of Pb loss events over the entire zircon data set identified a Middle Ordovician alteration event at ~470 Ma in the Archean zircon population from Yilgarn Craton rocks, synchronous to denudation and cooling that preceded the erosion of the Archean Yilgarn Craton and a Late Cretaceous Pb loss event that occurred after the breakup of Greater India and Australia. The ~470 Ma Pb loss age suggests that the intracratonic rift was initiated in the Early Paleozoic after the Kuunga Orogeny.

Overall, we argue that the complexity of zircon provenance and variations in zircon age spectra in the Tumblagooda Sandstone reflect the diversity of depositional environments in a highly dynamic rift basin environment, for which basin-wide stratigraphical correlations may be problematic. Finally, we show that detrital zircon studies greatly benefit from stratigraphically dense sampling intervals, particularly at the base of highly dynamic depositional environments such as continental red beds, to adequately represent provenance and rift basin architecture.

Acknowledgments

VM gratefully acknowledges the financial support by the Geological Survey of Western Australia (GSWA) through the Exploration Incentive Scheme (Royalties for Regions). Staff of GSWA core library are thanked for their assistance regarding drill core preparation, sampling, and scanning of cores with the HyLogger™ system. Carsten Laukamp (CSIRO Perth) and Paul Duuring (GSWA) are thanked for advice on hyperspectral data interpretations. Janet Muhling and Peter Duncan are thanked for technical assistance with the scanning electron microscope at the Centre for Microscopy, Characterization and Analysis facilities (The University of Western Australia). We would also like to thank Roger Hocking (GSWA) for guiding a field trip to the Murchison Gorge and helping to collect samples from the type sections. Paul Morris (GSWA) is thanked for assisting in the collection of whole rock geochemistry data. Klaus Gessner (GSWA) and Uri Shaanan (The University of Queensland) are thanked for thorough reviews of earlier versions of the manuscript. Anna Ksienzyk, an anonymous reviewer, and Associate Editor Andrew Carter are thanked for helpful comments and suggestions. Lena Hancock and Yongjun Lu publish with permission of the Executive Director of GSWA. GeoHistory Facility Instruments were funded via an Australian Geophysical Observing System grant provided to AuScope Limited by the AQ44 Australian Education Investment Fund program. This is contribution 1009 from the ARC Centre of Excellence for Core to Crust Fluid Systems (http://www.ccfs.mq.edu.au). All relevant data used in this study are attached as part of the supporting information.

References

Allen, H. J., & Trinajstic, K. (2017). An Early Devonian fish fauna from an unnamed sandstone in Wendy 1 drillhole, northern Perth Basin, Geological Survey of Western Australia, Paleontology Report 2017/1, pp. 1–4.

Andersen, T. (2005). Detrital zircons as tracers of sedimentary provenance: Limiting conditions from statistics and numerical simulation. *Chemical Geology*, *216*(3-4), 249–270. https://doi.org/10.1016/j.chemgeo.2004.11.013

Birnbaum, Z. W. (1952). Numerical tabulation of the distribution of Kolmogorov's statistic for finite sample size. *Journal of the American Statistical Association*, *47*(259), 425–441. https://doi.org/10.1080/01621459.1952.10501182

Boger, S. D. (2011). Antarctica—Before and after Gondwana. *Gondwana Research*, *19*(2), 335–371. https://doi.org/10.1016/j.gr.2010.09.003

Bruguier, O., Bosch, D., Pidgeon, R. T., Byrne, D. I., & Harris, L. B. (1999). U-Pb chronology of the Northampton Complex, Western Australia—Evidence for Grenvillian sedimentation, metamorphism and deformation and geodynamic implications. *Contributions to Mineralogy and Petrology*, *136*(3), 258–272. https://doi.org/10.1007/s004100050537

Byrne, D. R. (1997). Petrology, structural geology and tectonic history of the Northampton Complex, Western Australia, The University of Western Australia, Perth, PhD thesis.

Byrne, D. R., & Harris, L. B. (1993). Structural controls on the base-metal vein deposits of the Northampton Complex, Western Australia. *Ore Geology Reviews*, *8*(1-2), 89–115. https://doi.org/10.1016/0169-1368(93)90029-X

Cawood, P. A., & Nemchin, A. A. (2000). Provenance record of a rift basin: U/Pb ages of detrital zircons from the Perth Basin, Western Australia. *Sedimentary Geology*, *134*(3–4), 209–234. https://doi.org/10.1016/S0037-0738(00)00044-0

Cawood, P. A., Nemchin, A. A., Freeman, M. J., & Sircombe, K. (2003). Linking source and sedimentary basin: Detrital zircon record of sediment flux along a modern river system and implications for provenance studies. *Earth and Planetary Science Letters*, *210*(1–2), 259–268. https://doi.org/10.1016/S0012-821X(03)00122-5

Cawood, P. A., Johnson, M. R. W., & Nemchin, A. A. (2007). Early Palaeozoic orogenesis along the Indian margin of Gondwana: Tectonic response to Gondwana assembly. *Earth and Planetary Science Letters*, *255*(1-2), 70–84. https://doi.org/10.1016/j.epsl.2006.12.006

Clark, R. N., King, T. V., Klejwa, M., Swayze, G. A., & Vergo, N. (1990). High spectral resolution reflectance spectroscopy of minerals. *Journal of Geophysical Research*, *95*(B8), 12,653–12,680. https://doi.org/10.1029/JB095iB08p12653

Collins, A. S. (2003). Structure and age of the northern Leeuwin Complex, Western Australia: Constraints from field mapping and U–Pb isotopic analysis. *Australian Journal of Earth Sciences*, *50*(4), 585–599. https://doi.org/10.1046/j.1440-0952.2003.01014.x

Davies, N. S., & Gibling, M. R. (2010). Cambrian to Devonian evolution of alluvial systems: The sedimentological impact of the earliest land plants. *Earth-Science Reviews*, *98*(3–4), 171–200. https://doi.org/10.1016/j.earscirev.2009.11.002

Drew, J. H., Glen, A. G., & Leemis, L. M. (2000). Computing the cumulative distribution function of the Kolmogorov-Smirnov statistic. *Computational Statistics and Data Analysis*, *34*(1), 1–15. https://doi.org/10.1016/S0167-9473(99)00069-9

Embleton, B. J. J., & Schmidt, P. W. (1985). Age and significance of magnetizations in dolerite dykes from the Northampton Block, Western Australia. *Australian Journal of Earth Sciences*, *32*(3), 279–286. https://doi.org/10.1080/08120098508729330

Fedo, C. M., Sircombe, K. N., & Rainbird, R. H. (2003). Detrital zircon analysis of the sedimentary record. *Reviews in Mineralogy and Geochemistry*, *53*(1), 277–303. https://doi.org/10.2113/0530277

Fitzsimons, I. C. W. (2003). Proterozoic basement provinces of southern and southwestern Australia, and their correlation with Antarctica. *Geological Society, London, Special Publications*, *206*(1), 93–130. https://doi.org/10.1144/GSL.SP.2003.206.01.07

Goodge, J. W., Fanning, C. M., & Bennett, V. C. (2001). U–Pb evidence of ~1.7 Ga crustal tectonism during the Nimrod Orogeny in the Transantarctic Mountains, Antarctica: Implications for Proterozoic plate reconstructions. *Precambrian Research*, *112*(3-4), 261–288. https://doi.org/10.1016/S0301-9268(01)00193-0

Gorter, J. D., Nicoll, R. S., & Foster, C. N. (1994). Lower paleozoic facies in the Carnarvon Basin, Western Australia: Stratigraphy and hydrocarbon prospectivity. In *Proceedings of Petroleum Exploration Society of Australia*, (Vol. 2, pp. 373–396). Perth: The Sedimentary Basins of Western Australia.

Gregory, L. C., Meert, J. G., Bingen, B., Pandit, M. K., & Torsvik, T. H. (2009). Paleomagnetism and geochronology of the Malani Igneous Suite, Northwest India: Implications for the configuration of Rodinia and the assembly of Gondwana. *Precambrian Research*, *170*(1-2), 13–26. https://doi.org/10.1016/j.precamres.2008.11.004

Hall, L. S., Gibbons, A. D., Bernardel, G., Whittaker, J. M., Nicholson, C., Rollet, N., & Mǜller, R. D. (2013). Structural architecture of Australia's southwest continental margin and implications for Early Cretaceous basin evolution, West Australian Basins Symposium, 2013. Petroleum Exploration Society of Australia, Perth, WA, pp. 1-22.Hay, D. C., and T. J. Dempster, 2009, zircon alteration, formation and preservation in sandstones. *Sedimentology*, *56*, 2175–2191.

Herron, M. M. (1988). Geochemical classification of terrigenous sands and shales from core or log data. *Journal of Sedimentary Petrology*, *58*, 820–829.

Hocking, R. M. (1987). *Sedimentology and basin architecture of the Silurian Tumblagooda Sandstone, Perth-Carnarvon Basin, Western Australia*, (p. 126). New South Wales: University of New England.

Hocking, R. M. (1991). The Silurian Tumblagooda Sandstone, Western Australia, Geological Survey of Western Australia, Report 27, Perth, 124 pp.

Hunt, G. R. (1977). Spectral signatures of particulate minerals in the visible and near infrared. *Geophysics*, *42*(3), 501–513. https://doi.org/10.1190/1.1440721

Janssen, D. P., Collins, A. S., & Fitzsimons, I. C. W. (2003). Structure and tectonics of the Leeuwin Complex and Darling Fault Zone, southern Pinjarra Orogen, Western Australia—A field guide, Geological Survey of Western Australia, Record 2003/15, 33 pp.

Johnson, S. P. (2013). *The birth of supercontinents and the Proterozoic assembly of Western Australia* (p. 78). Perth: Geological Survey of Western Australia.

Johnson, S. P., Sheppard, S., Rasmussen, B., Wingate, M. T. D., Kirkland, C. L., Muhling, J. R., Fletcher, I. R., & Belousova, E. A. (2010). The Glenburgh Orogeny as a record of Paleoproterozoic continent-continent collision: Geological Survey of Western Australia, Geological Survey of Western Australia, Record 2010/5, 54 pp.

Kinny, P. D., Williams, I. S., Froude, D. O., Ireland, T. R., & Compston, W. (1988). Early Archaean zircon ages from orthogneisses and anorthosites at Mount Narryer, Western Australia. *Precambrian Research*, *38*(4), 325–341. https://doi.org/10.1016/0301-9268(88)90031-9

Kinny, P. D., Wijbrans, J. R., Froude, D. O., Williams, I. S., & Compston, W. (1990). Age constraints on the geological evolution of the Narryer Gneiss Complex, Western Australia. *Australian Journal of Earth Sciences*, *37*(1), 51–69. https://doi.org/10.1080/08120099008727905

Kriegsman, L. M., Möller, A., & Nelson, D. R. (1999). P–T–t path and detrital zircon geochronology of the Northampton Block, Western Australia: A Mesoproterozoic, collisional induced foreland rift. *Journal of Conference Abstracts*, *4*(1), 433.

Kruse, F. A. (1996). Identification and mapping of minerals in drill core using hyperspectral image analysis of infrared reflectance spectra. *International Journal of Remote Sensing*, *17*(9), 1623–1632. https://doi.org/10.1080/01431169608948728

Ksienzyk, A. K., Jacobs, J., Boger, S. D., Kosler, J., Sircombe, K. N., & Whitehouse, M. J. (2012). U-Pb ages of metamorphic monazite and detrital zircon from the Northampton Complex: Evidence of two orogenic cycles in Western Australia. *Precambrian Research*, *198-199*, 37–50. https://doi.org/10.1016/j.precamres.2011.12.011

Libby, W. G., de Laeter, J. R., & Myers, J. S. (1986). Geochronology of the Gascoyne Province, Western Australia Geological Survey, Report 50, p. 31.

Libby, W. G., De Laeter, J. R., & Armstrong, R. A. (1999). Proterozoic biotite Rb-Sr dates in the northwestern part of the Yilgarn Craton, Western Australia. *Australian Journal of Earth Sciences*, *46*(6), 851–860. https://doi.org/10.1046/j.1440-0952.1999.00749.x

Mandyczewsky, A. (1973). Stratigraphy and sedimentology of the Tumblagooda Sandstone, lower Murchison River area, Western Australia, The University of Western Australia, B.Sc. (Hons.) thesis.

Markwitz, V., & Kirkland, C. L. (2017). Source to sink zircon grain shape: Constraints on selective preservation and significance for Western Australian Proterozoic basin provenance. *Geoscience Frontiers*. https://doi.org/10.1016/j.gsf.2017.04.004

Markwitz, V., Kirkland, C. L., & Evans, N. J. (2017). Early Cambrian metamorphic zircon in the northern Pinjarra Orogen: Implications for the structure of the West Australian Craton margin. *Lithosphere*, *9*(1), 3–13. https://doi.org/10.1130/L569.1

McNamara, K. J. (2014). Early Paleozoic colonisation of the land: Evidence from the Tumblagooda Sandstone, Southern Carnarvon Basin, Western Australia. *Journal of the Royal Society of Western Australia*, *97*, 111–132.

McNamara, K. J., & Trewin, N. H. (1993). A euthycarcinoid arthropod from the Silurian of Western Australia. *Palaeontology*, *36*, 319–335.

McWhae, J. R. H., Playford, P. E., Lindner, A. W., Glenister, B. F., & Balme, B. E. (1956). The stratigraphy of western Australia. *Journal of the Geological Society of Australia*, *4*, 1–153.

Meert, J. G. (2003). A synopsis of events related to the assembly of eastern Gondwana. *Tectonophysics*, *362*(1-4), 1–40. https://doi.org/10.1016/S0040-1951(02)00629-7

Meert, J. G., & Van Der Voo, R. (1997). The assembly of Gondwana 800–550 Ma. *Journal of Geodynamics*, *23*(3-4), 223–235. https://doi.org/10.1016/S0264-3707(96)00046-4

Moecher, D. P., & Samson, S. D. (2006). Differential zircon fertility of source terranes and natural bias in the detrital zircon record: Implications for sedimentary provenance analysis. *Earth and Planetary Science Letters*, *247*(3-4), 252–266. https://doi.org/10.1016/j.epsl.2006.04.035

Morton, A. C. (1986). Dissolution of apatite in North Sea Jurassic sandstones: Implications for the generation of secondary porosity. *Clay Minerals*, *21*(4), 711–733. https://doi.org/10.1180/claymin.1986.021.4.16

Murakami, T., Chakoumakos, B. C., Ewing, R. C., Lumpkin, G. R., & Weber, W. J. (1991). Alpha-decay event damage in zircon. *American Mineralogist*, *76*, 1510–1532.
Myers, J. S. (1990). Precambrian tectonic history of the West Australian Craton and adjacent orogens. *Annual Review of Earth and Planetary Sciences*, *21*, 453–485.
Myers, J. S. (1995). The generation and assembly of an Archaean supercontinent: Evidence from the Yilgarn Craton, Western Australia. *Geological Society, London, Special Publications*, *95*(1), 143–154. https://doi.org/10.1144/GSL.SP.1995.095.01.09
Myers, J. S., Shaw, R. D., & Tyler, I. M. (1996). Tectonic evolution of Proterozoic Australia. *Tectonics*, *15*(6), 1431–1446. https://doi.org/10.1029/96TC02356
Nesbitt, H. W., & Young, G. M. (1982). Early Proterozoic climates and plate motions inferred from major element chemistry of lutites. *Nature*, *299*(5885), 715–717. https://doi.org/10.1038/299715a0
Ortega-Hernández, J., Legg, D. A., Tremewan, J., & Braddy, S. J. (2010). Euthycarcinoids. *Geology Today*, *26*(5), 195–198. https://doi.org/10.1111/j.1365-2451.2010.00770.x
Pettijohn, F. J. (1974). *Sedimentary rocks*. New York: Harper & Row.
Pettijohn, F., Portter, P., & Siever, R. (1972). *Sand and sandstone* (p. 618). New York, NY, USA: Springer.
Pidgeon, R. T. (2014). Zircon radiation damage ages. *Chemical Geology*, *367*, 13–22. https://doi.org/10.1016/j.chemgeo.2013.12.010
Playford, P. E., Cockbain, A. E., & Low, G. H. (1976). Geology of the Perth Basin, Western Australia, Geological Survey of Western Australia, Bulletin 124, 311 p.
Powell, C. M., & Pisarevsky, S. A. (2002). Late Neoproterozoic assembly of East Gondwana. *Geology*, *30*(1), 3–6. https://doi.org/10.1130/0091-7613(2002)030%3C0003:LNAOEG%3E2.0.CO;2
Powell, C. M., Li, Z. X., McElhinny, M. W., Meert, J. G., & Park, J. K. (1993). Paleomagnetic constraints on timing of the Neoproterozoic breakup of Rodinia and the Cambrian formation of Gondwana. *Geology*, *21*(10), 889–892. https://doi.org/10.1130/0091-7613(1993)021%3C0889:PCOTOT%3E2.3.CO;2
Reimink, J. R., Davies, J. H. F. L., Waldron, J. W. F., & Rojas, X. (2016). Dealing with discordance: A novel approach for analysing U–Pb detrital zircon datasets. *Journal of the Geological Society*, *173*(4), 577–585. https://doi.org/10.1144/jgs2015-114
Retallack, G. J. (2009). Cambrian, Ordovician and Silurian pedostratigraphy and global events in Australia. *Australian Journal of Earth Sciences*, *56*(4), 571–586. https://doi.org/10.1080/08120090902806321
Richards, J. R., Blockley, J. G., & De Laeter, J. R. (1985). Rb-Sr and Pb isotope data from the Northampton Block, Western Australia. *Proceedings of the Australian Institute of Mining & Metallurgy*, *290*, 43–55.
Roser, B. P., & Korsch, R. J. (1986). Determination of tectonic setting of sandstone-mudstone suites using content and ratio. *The Journal of Geology*, *94*(5), 635–650. https://doi.org/10.1086/629071
Roser, B. P., Cooper, R. A., Nathan, S., & Tulloch, A. J. (1996). Reconnaissance sandstone geochemistry, provenance, and tectonic setting of the lower Paleozoic terranes of the West Coast and Nelson, New Zealand. *New Zealand Journal of Geology and Geophysics*, *39*(1), 1–16. https://doi.org/10.1080/00288306.1996.9514690
Schmidt, P. W., & Embleton, B. J. J. (1990). The palaeomagnetism of the Tumblagooda Sandstone, Western Australia: Gondwana Palaeozoic apparent polar wandering. *Physics of the Earth and Planetary Interiors*, *64*(2-4), 303–313. https://doi.org/10.1016/0031-9201(90)90045-Y
Shaanan, U., & Rosenbaum, G. (2016). Detrital zircons as palaeodrainage indicators: Insights into southeastern Gondwana from Permian basins in eastern Australia. *Basin Research*. https://doi.org/10.1111/bre.12204
Sheppard, S., Rasmussen, B., Muhling, J. R., Farrell, T. R., & Fletcher, I. R. (2007). Grenvillian-aged orogenesis in the Palaeoproterozoic Gascoyne Complex, Western Australia: 1030–950 Ma reworking of the Proterozoic Capricorn Orogen. *Journal of Metamorphic Geology*, *25*(4), 477–494. https://doi.org/10.1111/j.1525-1314.2007.00708.x
Sircombe, K. N., & Hazelton, M. L. (2004). Comparison of detrital zircon age distribution by kernel functional estimation. *Sedimentary Geology*, *171*(1-4), 91–111. https://doi.org/10.1016/j.sedgeo.2004.05.012
Spaggiari, C. V., Kirkland, C. L., Smithies, R. H., Wingate, M. T. D., & Belousova, E. A. (2015). Transformation of an Archean craton margin during Proterozoic basin formation and magmatism: The Albany-Fraser Orogen, Western Australia. *Precambrian Research*, *266*, 440–466. https://doi.org/10.1016/j.precamres.2015.05.036
Spencer, C. J., & Kirkland, C. L. (2016). Visualizing the sedimentary response through the orogenic cycle: A multidimensional scaling approach. *Lithosphere*, *8*(1), 29–37. https://doi.org/10.1130/L479.1
Taylor, R. J. M., Kirkland, C. L., & Clark, C. (2016). Accessories after the facts: Constraining the timing, duration and conditions of high-temperature metamorphic processes. *Lithos*, *264*, 239–257. https://doi.org/10.1016/j.lithos.2016.09.004
Thomas, W. A. (2011). Detrital-zircon geochronology and sedimentary provenance. *Lithosphere*, *3*(4), 304–308. https://doi.org/10.1130/RF.L001.1
Trewin, N. H. (1993). Controls on fluvial deposition in mixed fluvial and aeolian facies within the Tumblagooda Sandstone (Late Silurian) of Western Australia. *Sedimentary Geology*, *85*(1-4), 387–400. https://doi.org/10.1016/0037-0738(93)90094-L
Trewin, N. H., & McNamara, K. J. (1995). Arthropods invade the land: Trace fossils and palaeoenvironments of the Tumblagooda Sandstone (? Late Silurian) of Kalbarri, Western Australia. *Transactions of the Royal Society of Edinburgh: Earth Sciences*, *85*, 177–210.
Vavra, G., Gebauer, D., Schmid, R., & Compston, W. (1996). Multiple zircon growth and recrystallization during polyphase Late Carboniferous to Triassic metamorphism in granulites of the Ivrea zone (Southern Alps): An ion microprobe (SHRIMP) study. *Contributions to Mineralogy and Petrology*, *122*(4), 337–358. https://doi.org/10.1007/s004100050132
Veevers, J. J., James, J., & Conaghan, P. J. (1984). *Phanerozoic earth history of Australia*. USA: Oxford University Press.
Veevers, J. J., Saeed, A., Belousova, E. A., & Griffin, W. L. (2005). U–Pb ages and source composition by Hf-isotope and trace-element analysis of detrital zircons in Permian sandstone and modern sand from southwestern Australia and a review of the paleogeographical and denudational history of the Yilgarn Craton. *Earth-Science Reviews*, *68*(3-4), 245–279. https://doi.org/10.1016/j.earscirev.2004.05.005
Vermeesch, P. (2013). Multi-sample comparison of detrital age distributions. *Chemical Geology*, *341*, 140–146.
Vermeesch, P., Resentini, A., & Garzanti, E. (2016). An R package for statistical provenance analysis *Sedimentary Geology*, *336*, 14–25.
Walderhaug, O., & Porten, K. W. (2007). Stability of detrital heavy minerals on the Norwegian continental shelf as a function of depth and temperature. *Journal of Sedimentary Research*, *77*(12), 992–1002. https://doi.org/10.2110/jsr.2007.091
Wang, Y., Zhang, F., Fan, W., Zhang, G., Chen, S., Cawood, P. A., & Zhang, A. (2010). Tectonic setting of the South China Block in the early Paleozoic: Resolving intracontinental and ocean closure models from detrital zircon U-Pb geochronology. *Tectonics*, *29*(6), TC6020. https://doi.org/10.1029/2010TC002750
Went, D. J. (2013). Quartzite development in early Palaeozoic nearshore marine environments. *Sedimentology*, *60*(4), 1036–1058. https://doi.org/10.1111/sed.12016

Wiemer, D., Allen, C. M., Murphy, D. T., & Kinaev, I. (2017). Effects of thermal annealing and chemical abrasion on ca. 3.5 Ga metamict zircon and evidence for natural reverse discordance: Insights for U-Pb LA-ICP-MS dating. *Chemical Geology*, *466*, 285–302. https://doi.org/10.1016/j.chemgeo.2017.06.019

Wingate, M. T. D., & Mory, A. J. (2015). 181250: Quartz sandstone, Coburn 1, Geological Survey of Western Australia, Geochronology Record 1268, 5 p.

Wingate, M. T. D., Hocking, R. M., & Mory, A. J. (2015). 181105: Quartz sandstone, Rainbow Valley, Geological Survey of Western Australia, Geochronology Record 1266, 6 p.